Electronic Supplementary Information

Multifunctional Nanomicelles Constructed by Aggregation and De-aggregation Strategy for Magnetic Resonance/NIR II Fluorescence Imaging guided Type I Photodynamic Therapy

Lirong Wang,[a,b#] Ji Qi,[d#] Ke Zhang,[e] Zeyan Zhuang,[a,b] Keke Ding,[f] Xu Chen,[a,b] Hong Shan,[e] Dan Ding,[d] Anjun Qin,*[a,b] Ben Zhong Tang[b,c,g]

[a] State Key Laboratory of Luminescent Materials and Devices, Guangdong Provincial Key Laboratory of Luminescence from Molecular Aggregates, South China University of Technology, Guangzhou 510640, China. E-mail:msqinaj@scut.edu.cn.

[b] Center for Aggregation-Induced Emission, AIE Institute, South China University of Technology, Guangzhou 510640, China.

[c] School of Science and Engineering, Shenzhen Institute of Aggregate Science and Engineering, The Chinese University of Hong Kong, Shenzhen, 518172, Guangdong, China.

[d] State Key Laboratory of Medicinal Chemical Biology, College of Life Sciences, Nankai University, Tianjin 300071, China.

[e] Center for Interventional Medicine, The Fifth Affiliated Hospital, Sun Yat-sen University, Zhuhai 519000, China.

[f] Department of Urology, The First Affiliated Hospital of Soochow University, Suzhou 215006, China.

[g] Hong Kong Branch of Chinese National Engineering Research Centre for Tissue Restoration and Reconstruction, The Hong Kong University of Science & Technology, Clear Water Bay, Kowloon, Hong Kong, China.

Equipment and Method

^{1}H and ^{13}C NMR spectra were measured on a Bruker AV 500 spectrometer. UV-vis absorption spectra were measured on a Shimadzu UV-2600 spectrophotometer. Photoluminescence spectra were recorded on a Horiba Fluoromax-4 spectrofluorometer. Photoluminescence (PL) quantum yields were measured using a Hamamatsu absolute PL quantum yield spectrometer C11347 Quantaurus_QY. The Electron paramagnetic resonance (EPR) measurements were carried out on Bruker ELEXSYS-II E500 in X-band. Confocal laser scanning microscope (CLSM) characterization was conducted with a Zeiss LSM 710 (Germany) confocal laser scanning biological microscope. The absorbance for MTT analysis was recorded on a Thermo Fisher microplate reader (USA) at a wavelength of 490 nm. The element analysis of Gd was also carried out by inductively coupled plasma mass spectroscopy. The morphology and structure of TGdTT NMs were characterized by transmission electron microscopy (TEM) using a JEOL JEM-2100 transmission electron microscope. The dynamic light scattering (DLS) measurements were performed on a Malvern Zetasizer nano ZS instrument. The T_1 relaxation time measurements were performed on 0.5 T NMI20-Analyst NMR Analyzing & imaging system (Niumag Corporation, Shanghai, China), *in vivo* MR imaging was performed on a 9.4 T MRI scanner (Bruker Biospin Corporation, Ettlingen，Germany). *In vivo* fluorescence imaging was carried out on Full Spectrum Animal In Vivo Imaging System AniView Phoenix 600 (Guangzhou Biolight Biotechnology Co., Ltd).

The ground- and excited-state geometries were optimized using density functional theory (DFT) and time-dependent DFT (TD-DFT) method, respectively, at the level of M06-2X/6-311G(d,p), performed by the Gaussian 16 software package. No symmetry constraint was applied for optimization. The spin-orbit coupling (SOC) value was calculated using TD-DFT method at the level of M06-2X/def2-TZVP, performed by ORCA 4.1. The vertical electronic affinity (VEA) was calculated using DFT method at the level of M06-2X/6-311+G(d,p), performed by Gaussian 16 software package.

PL Quantum yields of TQ-TPA NMs and TGdTT NMs

The fluorescence quantum yields of TGdTT NMs and TQ-TPA NMs in water were measured using the relative method.[1] ICG was chosen as the reference dye with quantum yield of 13% in DMSO. Then, different concentrations of ICG in DMSO was prepared and further measured the absorbance (A) ($A<0.1$, to prevent re-absorption) and the PL spectra at 765 nm. Following the above conditions, the A and the PL spectra at 765 nm of TGdTT NMs and TQ-TPA NMs were measured. Based on the PL spectra, the integrated fluorescence intensity (D) of ICG, TGdTT NMs and TQ-TPA NMs

corresponding with suitable A were recorded respectively. A graph of D versus A was plotted to determine the gradient (G). Quantum yields (Φ) of TGdTT NMs and TQ-TPA NMs were calculated from $\Phi_s = \Phi_r\left(\frac{G_s}{G_r}\right)\left(\frac{I(\lambda_r)}{I(\lambda_s)}\right)\left(\frac{n_s}{n_r}\right)^2$. The subscripts "r" and "s" refer to the reference dye and the sample, respectively; n is the refractive index of the solvent; and $I(\lambda)$ is the relative intensity of the exciting light at wavelength λ (765 nm).

Total ROS detection

The ROS generation of TQ-TPA NMs, TGdTT NMs, and Ce6 was detected by 2,7-dichlorodihydrofluorescein (DCFH). Briefly, 0.5 mL 2,7-dichlorodihydrofluorescein diacetate (DCFH-DA) in ethanol (1 mM) was added to 2 mL NaOH (10 mM) and allowed to stir at room temperature for 30 min. Then the hydrolysate was diluted with 10 mL of 1 × PBS to obtain the hydrolyzed DCFH with the concentration of 40 μM, which was kept in dark for use. Then, 10 μM DCFH aqueous solution and predetermined photosensitizer were added into 2 mL water solution for the PL spectra measurement under 660 nm laser irradiation at different intervals. The excitation wavelength was 488 nm and emission was collected from 510 to 600 nm.

Hydroxyl radical (•OH) detection

The •OH generation was probed by hydroxyphenyl fluorescein (HPF). HPF (5 μM, stock solution: 5 mM in DMF) mixed with or without 10 μM TQ-TPA NMs in the PBS aqueous solution was irradiated with 660 nm laser (0.3 W/cm^2) at different intervals. Additionally, 0.5, 2, 5, 10 μM BSA aqueous solution as the reductive substrates were added into the mixing solution of TQ-TPA NMs and HPF with the same experimental conditions, respectively. The fluorescence signal of HPF was monitored in a range of 500-550 nm with the excitation wavelength at 480 nm and the fluorescence intensity at 514 nm was recorded to indicate the •OH generation rate.

Singlet oxygen ($^1O_2$) detection

The $^1O_2$ generation of photosensitizer was evaluated by 9,10-anthracenediyl-bis(methylene) dimalonic acid (ABDA). ABDA (50 μM) mixed with or without 10 μM

TQ-TPA NMs in water was irradiated with 660 nm laser (0.3 W/cm^2) at different intervals. The absorbance of ABDA at 378 nm was recorded at each irradiation time.

Electron paramagnetic resonance (EPR) for Type I ROS detection

EPR analysis was carried out to monitor the generation of Type I ROS using 5,5-dimethyl-1-pyrroline *N*-oxide (DMPO) as spin-trap agent. 0.1M DMPO PBS solution was added 30 μM TQ-TPA NMs or TGdTT NMs. The spectrum was monitored in a range of 3000-4000 G after the solution was irradiated with 660 nm laser (0.3 mW/cm^2) for 3 min.

T_1 Relaxivity Study

The T_1 relaxation time of TGdTT NMs, 2TPE-Gd NMs, 2TPE-Gd, and Gd-DOTA were measured at 0.5 T MRI scanner with the Gd(III) concentration of 0.4, 0.2, 0.1, 0.05, and 0.025 mM, respectively. Then, the values of r_1 were calculated through the curve fitting of relaxation rates (s^{-1}) versus the Gd(III) concentration (mM).

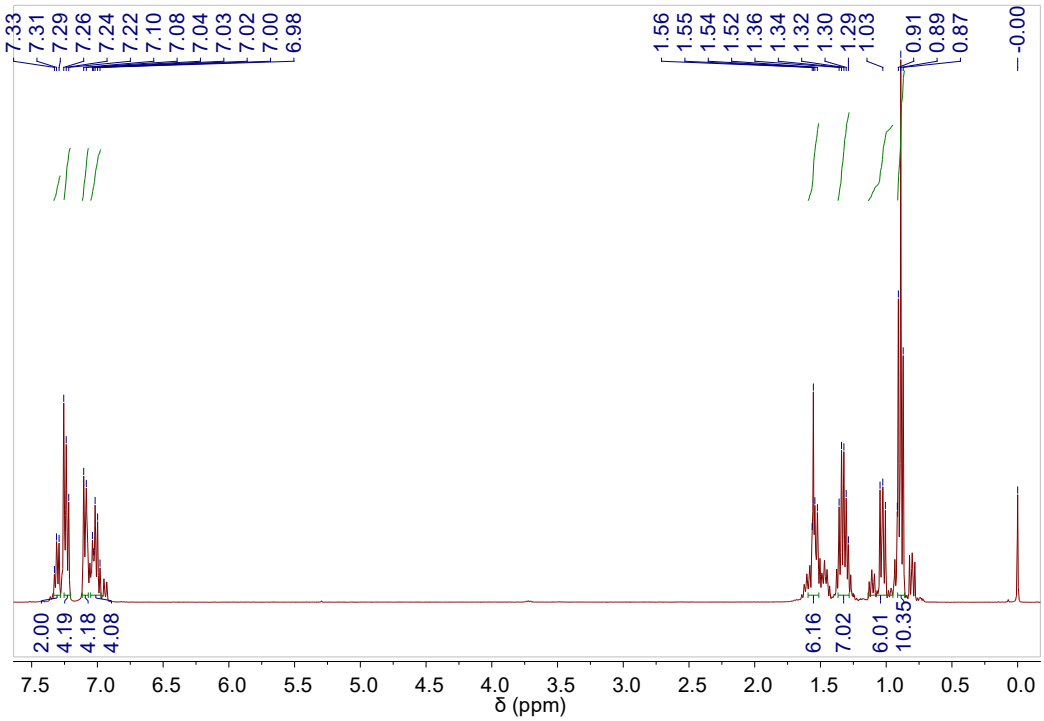

Fig. S1. ^{1}H NMR spectrum of **4** in $CDCl_3$.

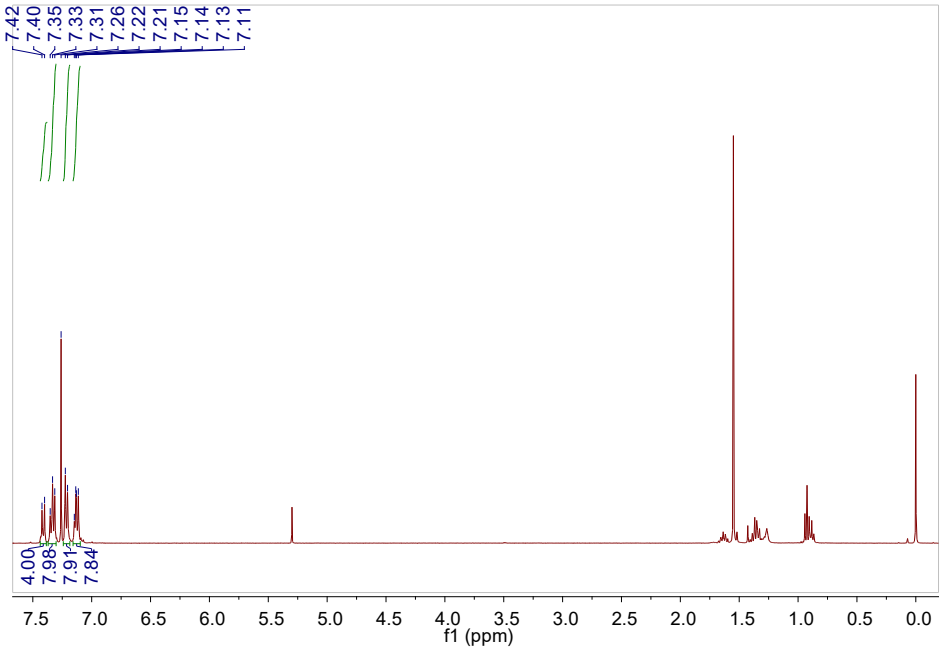

Fig. S2. ^{1}H NMR spectrum of **5** in $CDCl_3$.

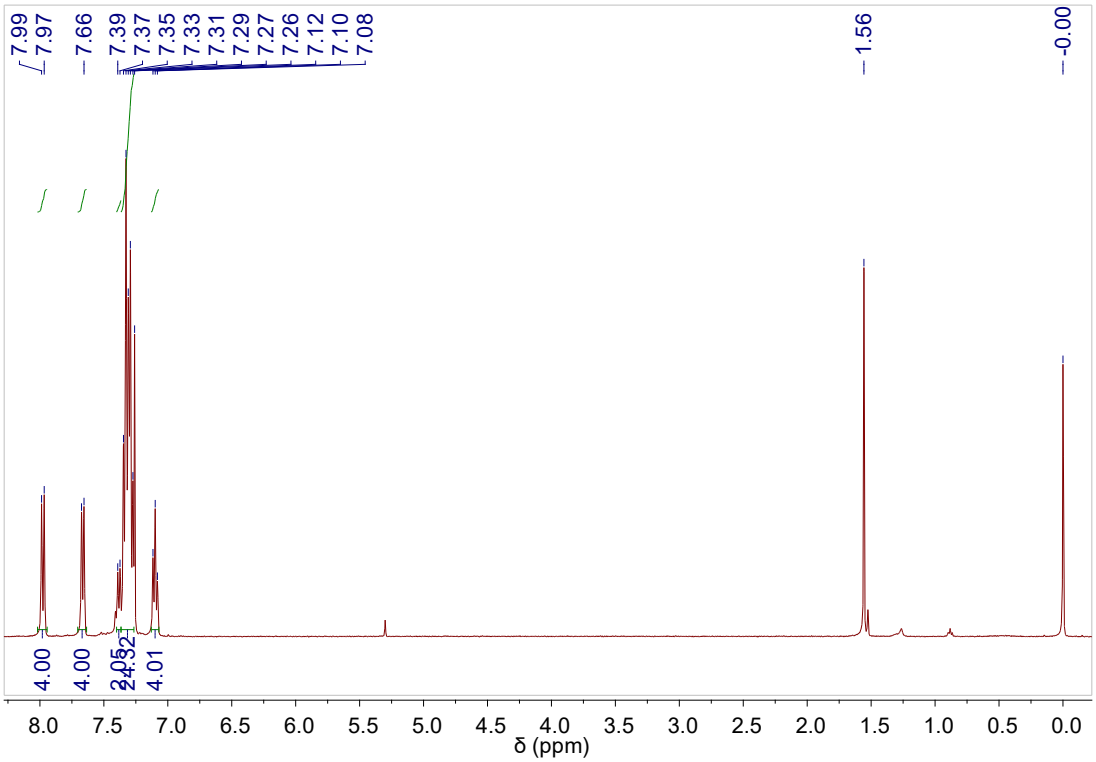

Fig. S3. ^{1}H NMR spectrum of TPA-TQ in $CDCl_3$.

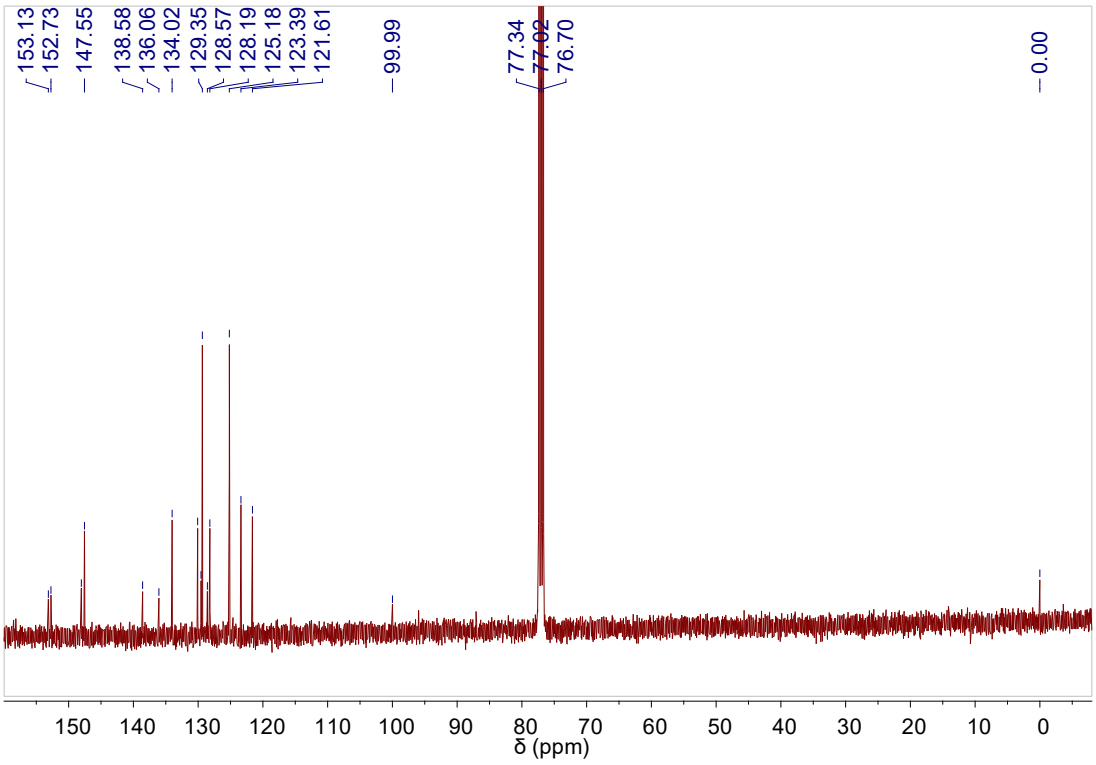

Fig. S4. ^{13}C NMR spectrum of TPA-TQ in $CDCl_3$.

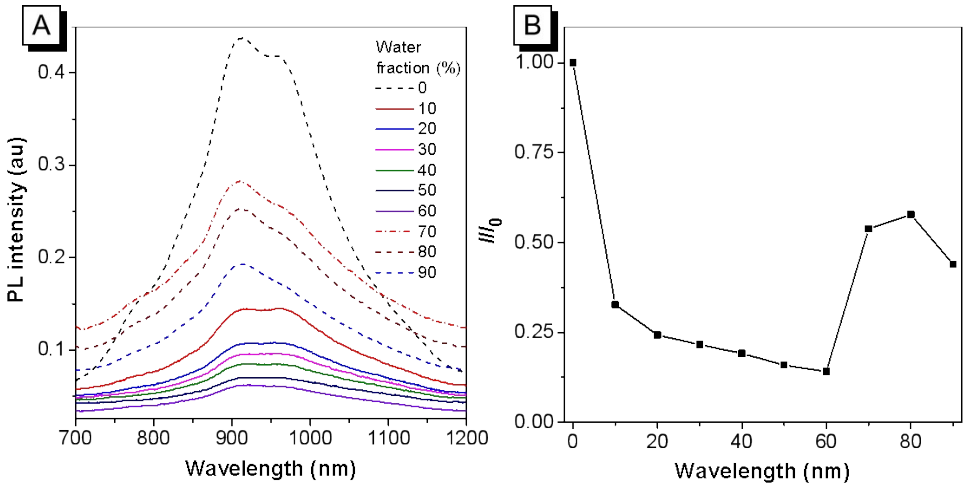

Fig. S5. (A) PL spectra of TQ-TPA in THF/water mixtures with different water fractions (f_w). (B) Plots of the relative emission intensity of TQ-TPA versus water fraction. I_0 and I are the peak values of PL intensities of TQ-TPA (10 μM) in THF and THF/water mixtures with different f_w, respectively.

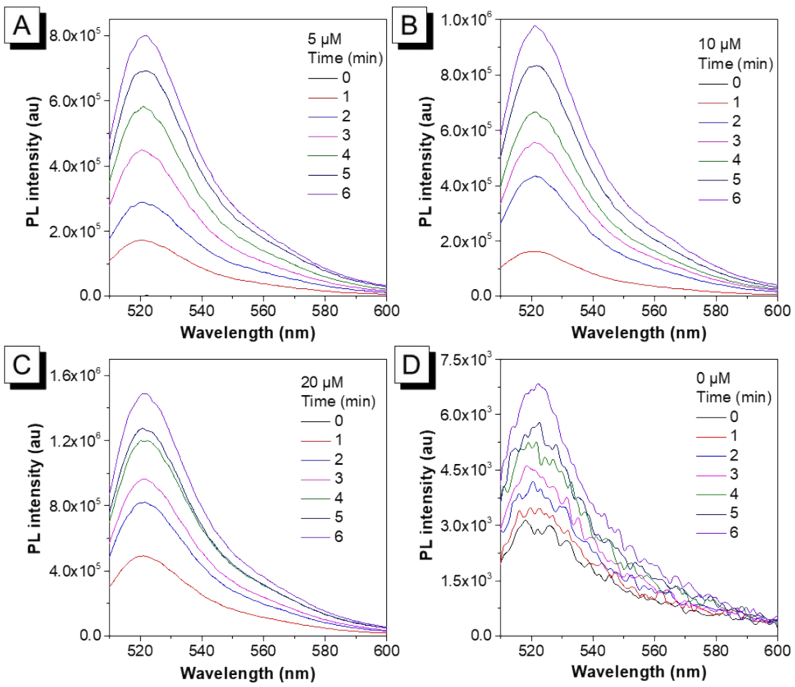

Fig. S6. PL spectra of DCFH upon incubation with TQ-TPA NMs with concentration of (A) 5 μM, (B) 10 μM, (C) 20 μM, and (D) 0 μM under 660 nm laser irradiation (0.3 W/cm^2) at different time.

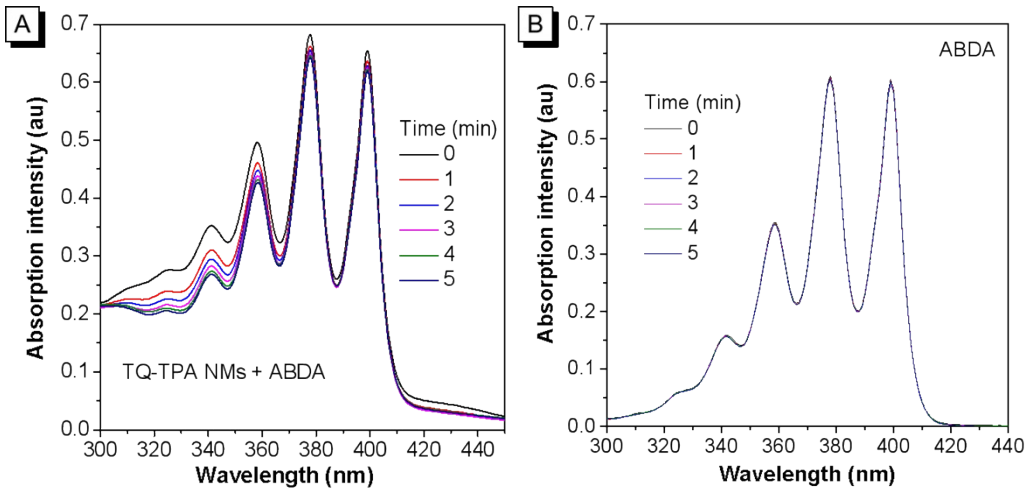

Fig. S7. Absorption spectra of ABDA with (A) or without (B) TQ-TPA NMs under 660 nm laser irradiation (0.3 W/cm^2) at different time.

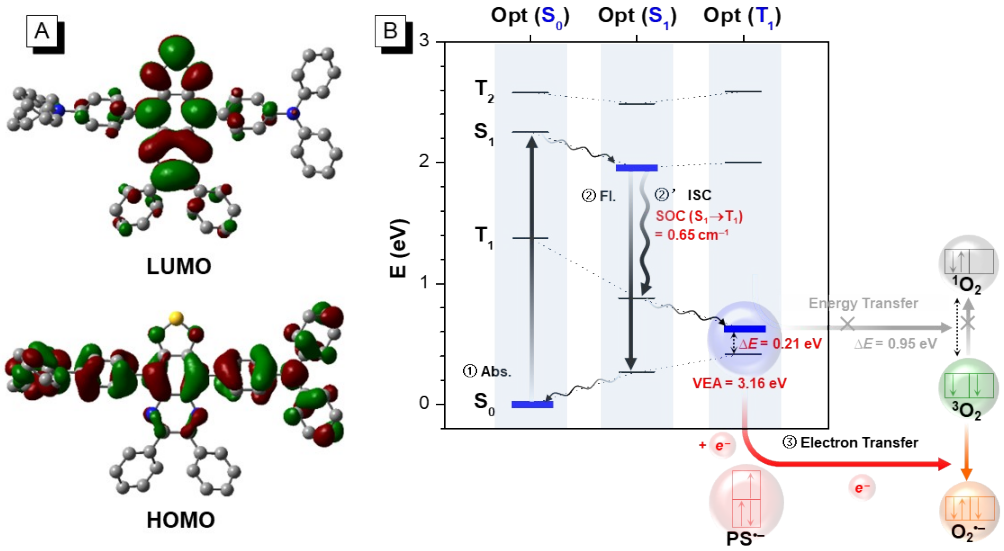

Fig. S8. (A) Contours of HOMO and LUMO at the optimized S_1 state structures of TQ-TPA. (B) Calculated energy diagram and proposed ROS generating mechanism of TQ-TPA.

Scheme S1. Synthetic routes to 2TPE-Gd.

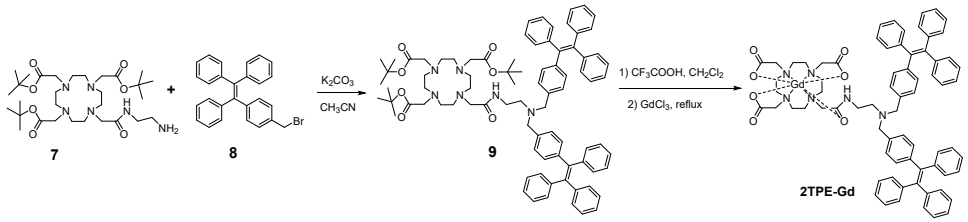

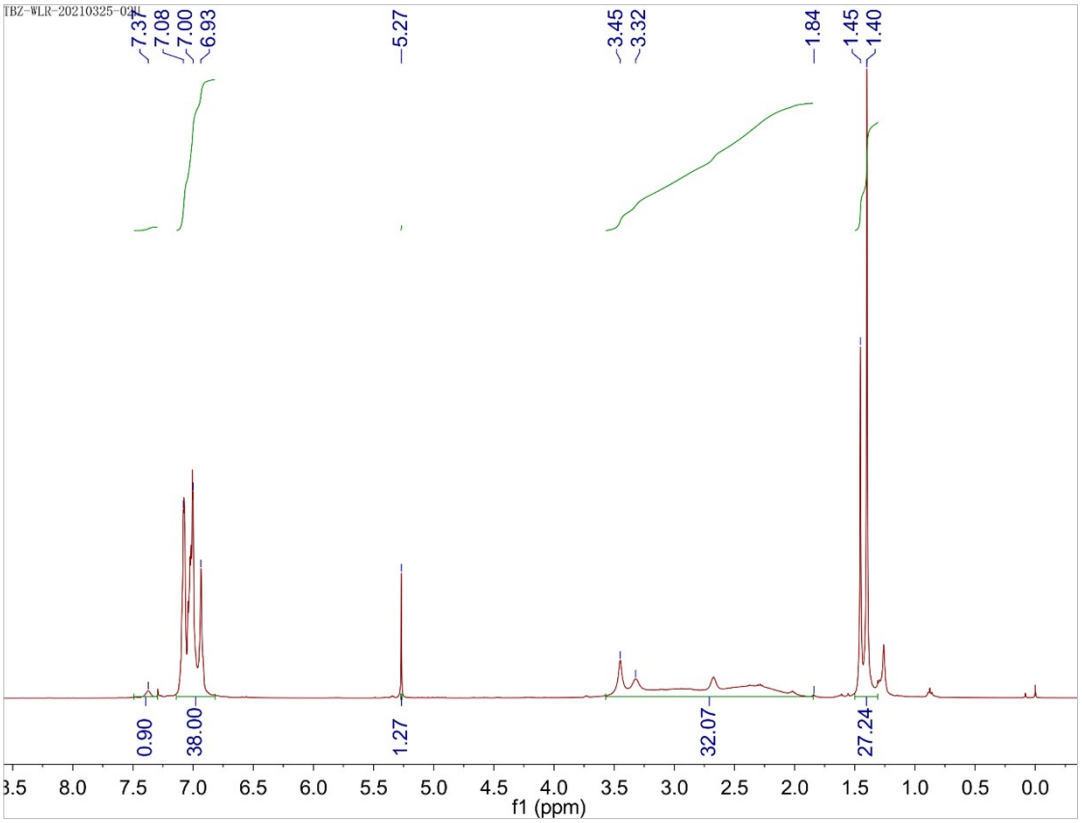

Fig. S9. ^{1}H NMR of compound **9** in $CDCl_3$.

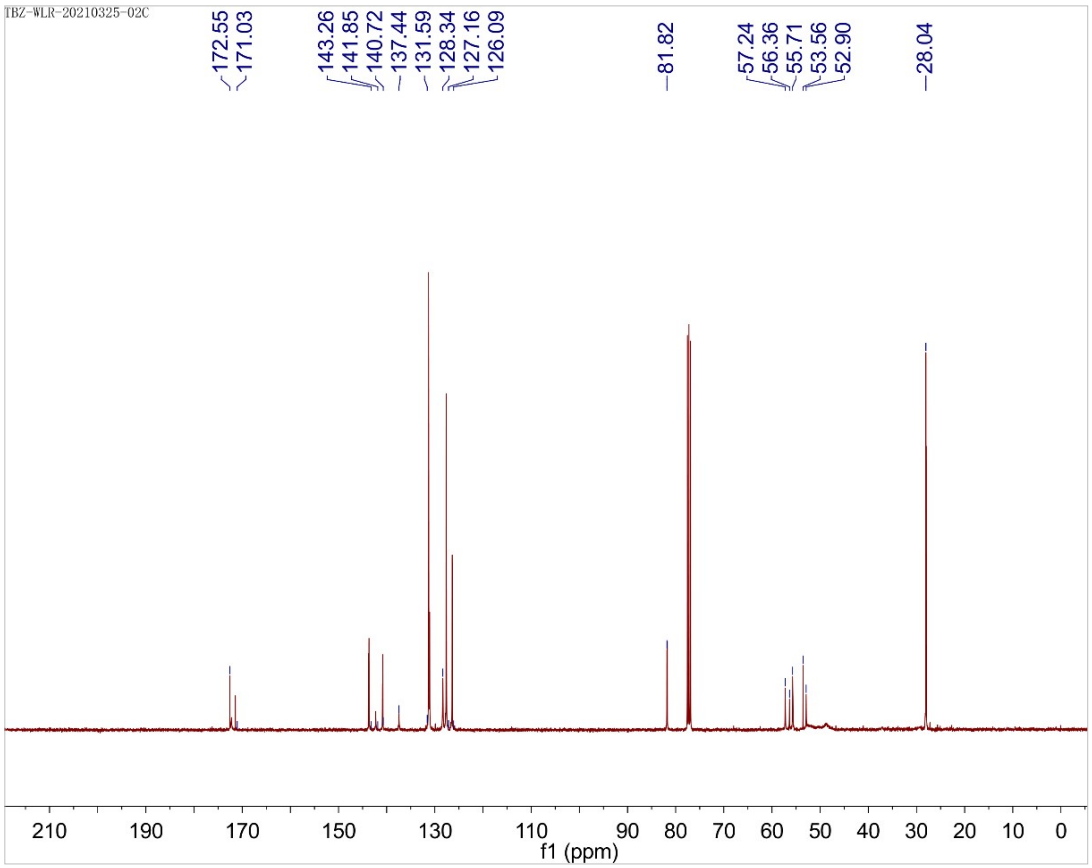

Fig. S10. ^{13}C NMR of compound **9** in $CDCl_3$.

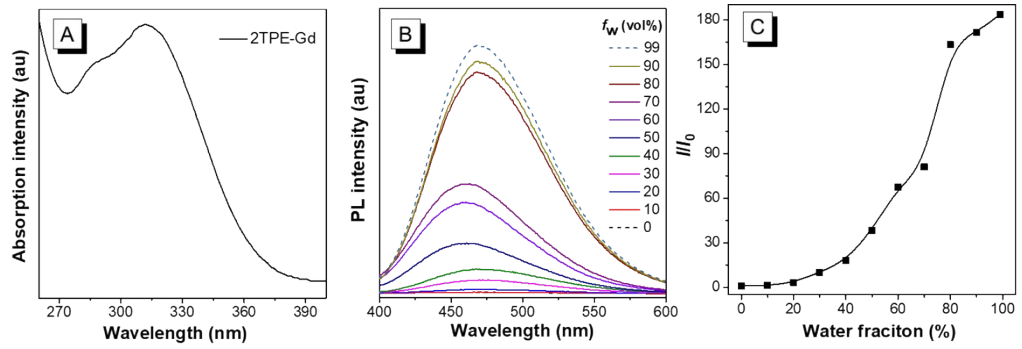

Fig. S11. (A) Absorption spectrum of 2TPE-Gd (10 μM) in THF. (B) Photoluminescence (PL) spectra of 2TPE-Gd (10 μM) in THF/water mixtures with different water fractions (f_w). (C) Plots of the relative emission intensity of 2TPE-Gd versus water fraction. I_0 and I are the PL intensities of 2TPE-Gd (10 μM) in THF and THF/water mixtures with different f_w, respectively.

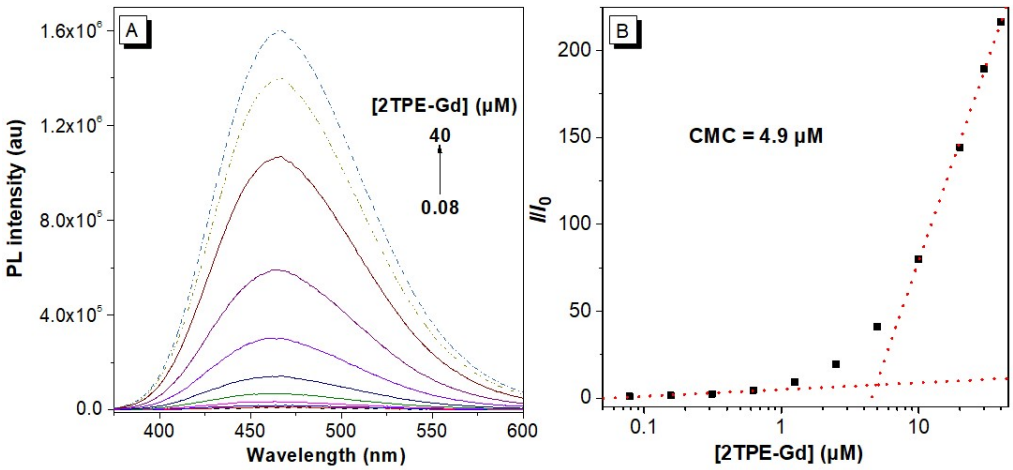

Fig. S12. The CMC of 2TPE-Gd. (A) PL spectra of 2TPE-Gd as the increasing concentration in aqueous solution. (B) Plot of the PL intensity versus the concentration of 2TPE-Gd.

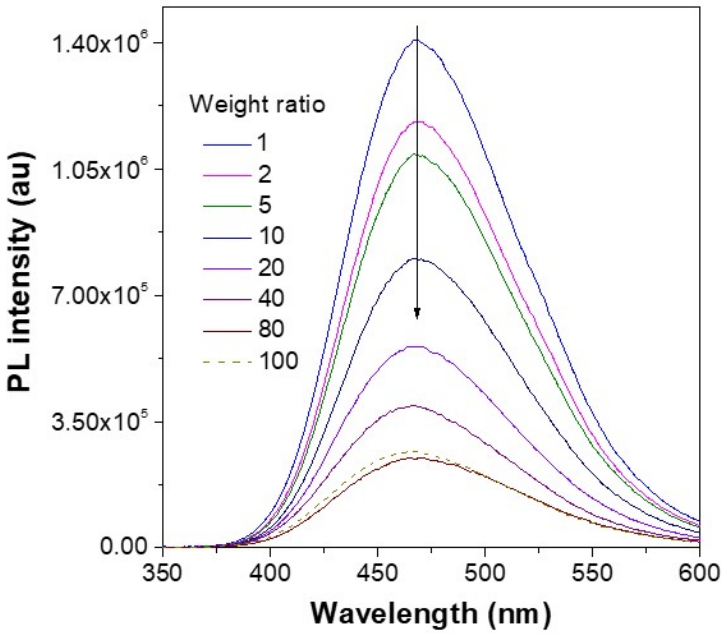

Fig. S13. PL spectra of 2TPE-Gd in the system of DSPE-PEG/2TPE-Gd with different weight ratio. The concentration of 2TPE-Gd was 10 μM.

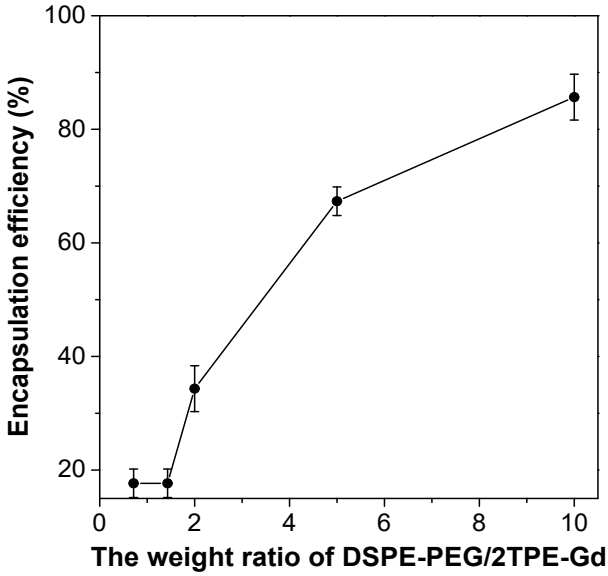

Fig. S14. The encapsulation efficiency (EE) of 2TPE-Gd in DSPE-PEG/2TPE-Gd system.

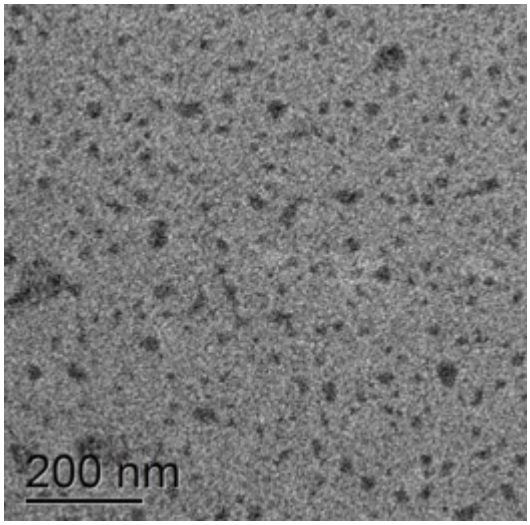

Fig. S15. The TEM image of 2TPE-Gd NMs.

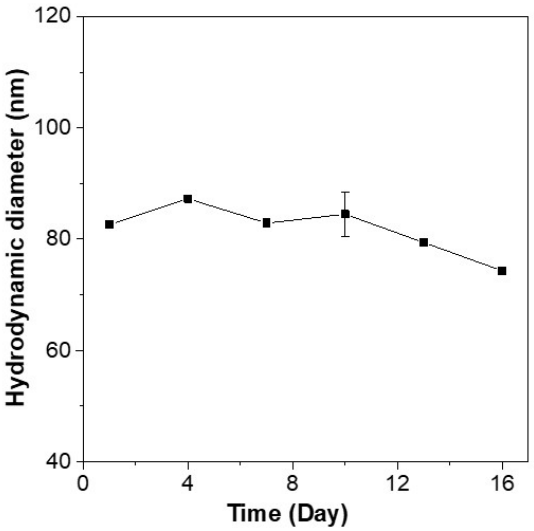

Fig. S16. The hydrodynamic diameter of TGdTT NMs measured by DLS.

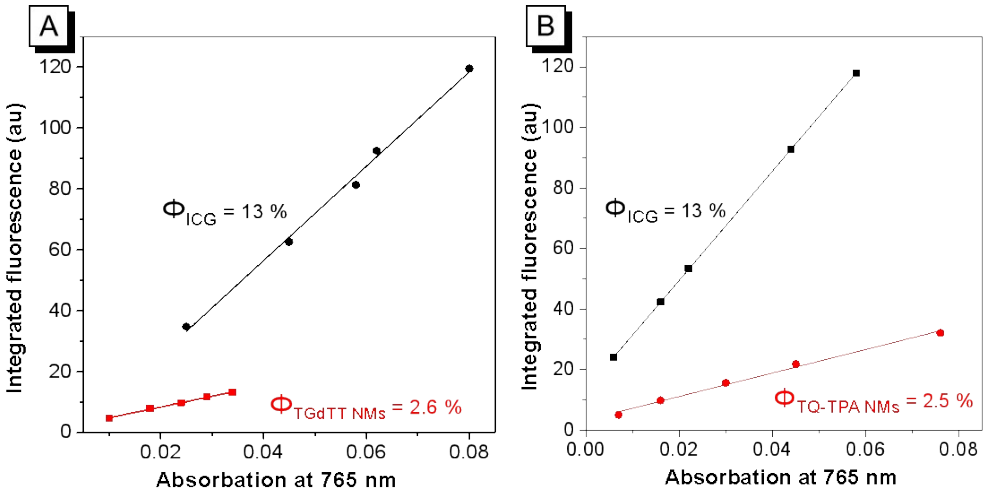

Fig. S17. The measurement of relative fluorescence quantum yield (Φ). (A) The fitted curves of absorption at 765 nm vs. integral area of emission of ICG in DMSO and TQ-TPA NMs in water, respectively. Taking the Φ_{ICG} as a reference, the calculated $\Phi_{TGdTT\ NMs}$ is about 2.5% (~3%). (B) The fitted curves of absorption at 765 nm vs. integral area of emission of ICG in DMSO and TQ-TPA NMs in water, respectively. Taking the Φ_{ICG} as a reference, the calculated $\Phi_{TQ\text{-}TPA\ NMs}$ is about 2.6% (~3%).

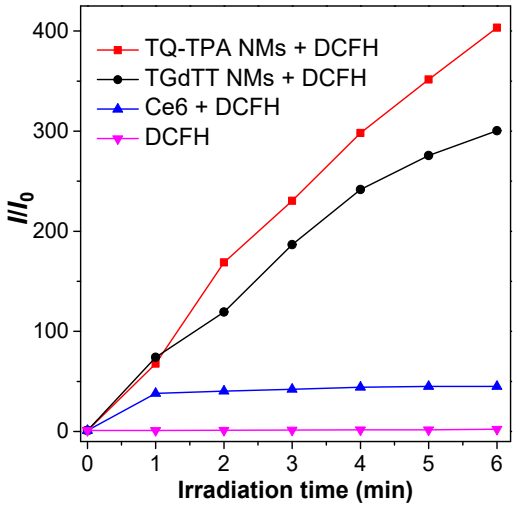

Fig. S18. Plots of the relative PL intensity of DCFH without or with addition of TQ-TPA NMs, TGdTT NMs, and Ce6 under 660 nm laser irradiation (0.3 W/cm^2), respectively.

Table S1. The relaxivities, sizes measured by TEM, hydration diameters (HD) measured by DLS of TGdTT NMs, 2TPE-Gd NMs, 2TPE-Gd, and Gd-DOTA, respectively .

Sample	r_1 ($mM^{-1}s^{-1}$) at 0.5 T	Size (nm) (By TEM)	HD (nm) (By DLS)
TGdTT NMs	32.5 ± 0.6	52.2 ± 10.2	91.3 ± 3.9
2TPE-Gd NMs	25.3 ± 0.8	37.2 ± 6.6	78.8 ± 5.4
2TPE-Gd	10.5 ± 0.6	No data	5.6 ± 0.4
Gd-DOTA	5.2 ± 0.2	No data	0.8 ± 0.03

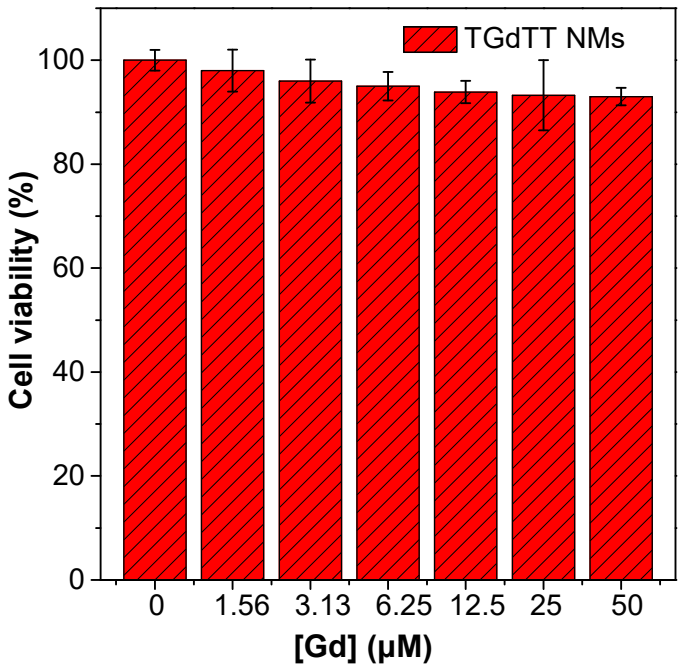

Fig. S19. Cell viability of 4T1 cells incubated with different concentration of TGdTT NMs incubated for 24 h. [Gd] = 0~50 μM.

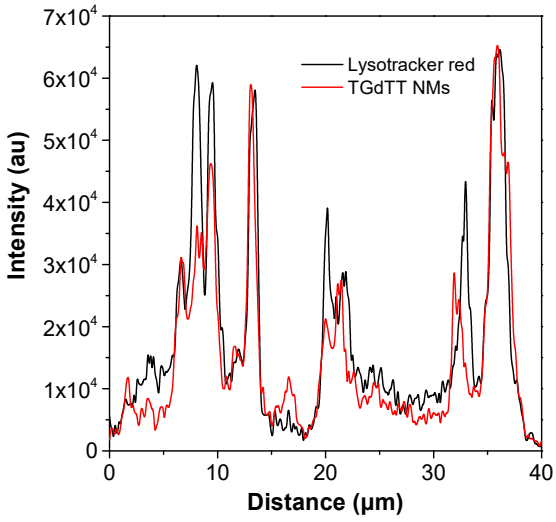

Fig. S20. Line analysis of TGdTT NMs with Lysotracker red was conducted after incubation with TGdTT NMs for 4 h.

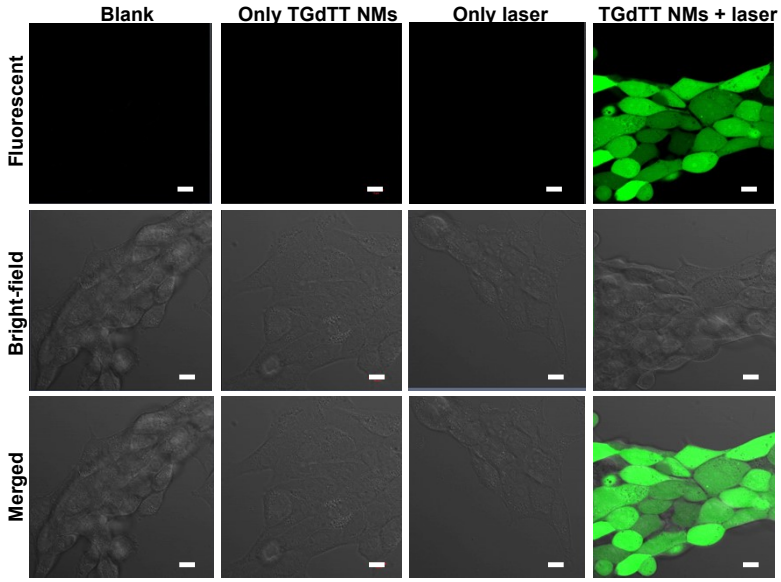

Fig. S21. Intracellular ROS level of 4T1 cells indicated by DCFH-DA after various treatment. Scale bar: 10 μm. Laser irradiation (660 nm, 0.3 W/cm^2, 5 min) was conducted when cells were incubated with TGdTT NMs (10 μM) for 12 h.

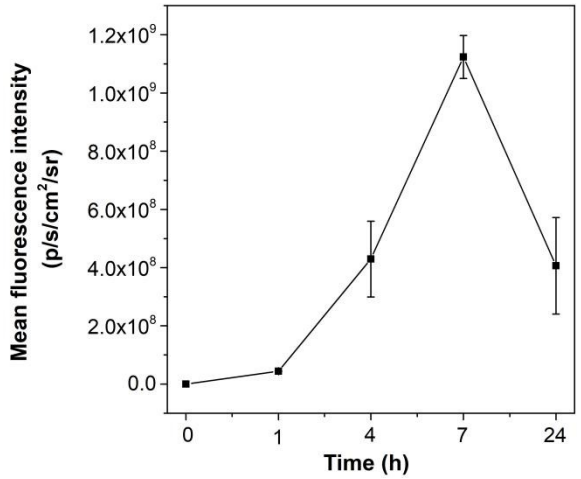

Fig. S22. The NIR II fluorescence intensity of the images in Fig. 5C.

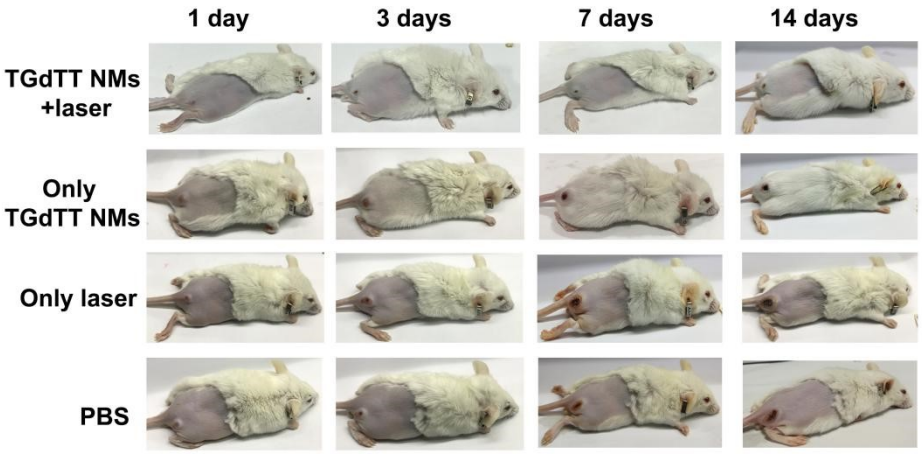

Fig. S23. Representative photos of 4T1 tumor-bearing mice of different groups during 14-day treatments.

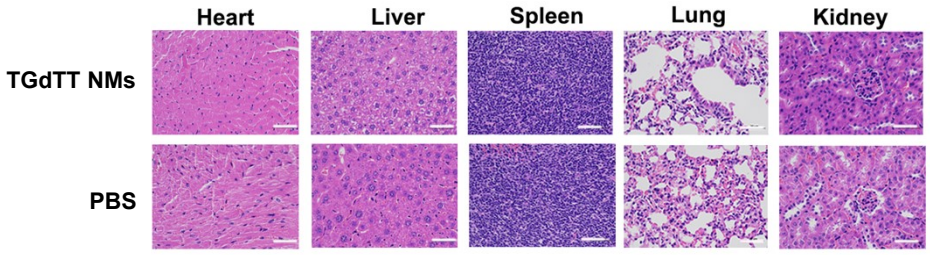

Fig. S24. H&E staining tissue sections from mice treated with TGdTT NMs and PBS. Scale bar: 50 μm.

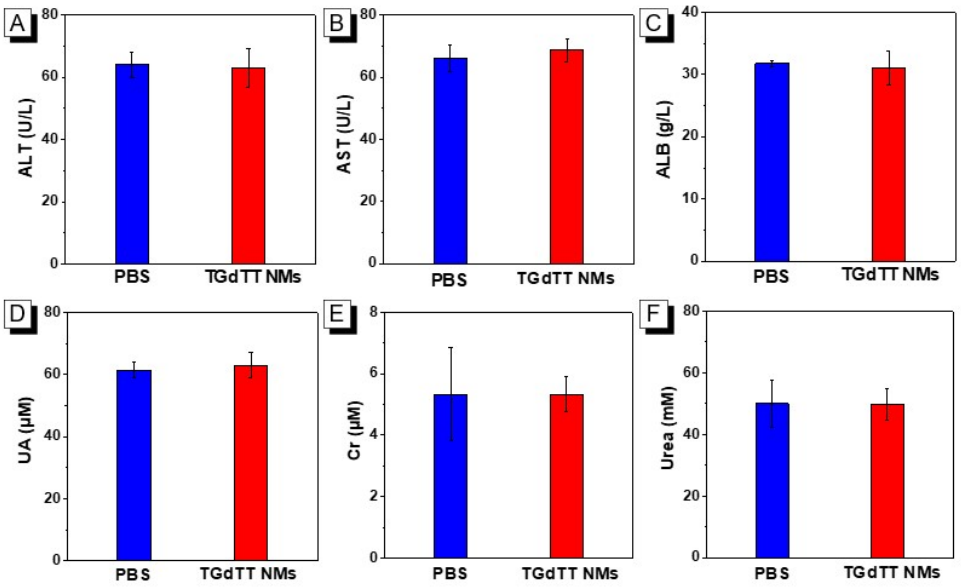

Fig. S25. Biosafety assessment of mice (n = 3/group) after injection of TGdTT NMs and PBS respectively. (A) ALT, (B) AST, and (C) ALB are liver function indices. (D) UV, (E) Cr, and (F) Urea are renal functions indices.

Reference

1. M. Luo, H. Shadnia, G. Qian, X. Du, D. Yu, D. Ma, J. S. Wright, and Z. Y. Wang, Rational design, synthesis, and optical properties of film-forming, near-infrared absorbing, and fluorescent chromophores with multidonors and large heterocyclic acceptors, *Chemistry*, 2009, **15**, 8902-8908.